Phase Structure and Morphology of Wollastonite-Reinforced Polypropylene Composites Modified With SEBS and SEBS-*g*-MA Elastomers

Iztok Švab,[1] Vojko Musil,[1] Tanja Jurkin,[2] Ivan Šmit[2]
[1] *University of Maribor, FEB Maribor, Institute of Technology, Razlagova 14, 2000 Maribor, Slovenia*

[2] *Ruđer Bošković Institute, Bijenička 54, 10002 Zagreb, Croatia*

Supermolecular structure of isotactic polypropylene/wollastonite/styrenic rubber block copolymers composites were studied as a function of elastomeric poly(styrene-*b*-ethylene-*co*-butylene-*b*-styrene) triblock copolymer (SEBS) and the SEBS grafted with maleic anhydride (SEBS-*g*-MA) content (from 0 to 20 vol%) by optical, scanning, and transmission electron microscopy, wide-angle X-ray diffraction and differential scanning calorimetry. Wollastonite particles disturbed the spherulitization of polypropylene matrix. Both elastomers affected the crystallization of polypropylene matrix mainly by solidification effect. Although SEBS-*g*-MA encapsulated wollastonite particles more expressive than SEBS forming thus core-shell morphology in higher extent, scanning electron micrographs indicated more constrained wollastonite particles in fractured surfaces of composites with SEBS elastomer. Moreover, SEBS-*g*-MA disorientated wollastonite particles and affected reorientation of the polypropylene crystallites stronger than SEBS elastomer. POLYM. ENG. SCI., 47:2145–2154, 2007.

INTRODUCTION

The intensive growth and use of particulate-filled polymer composites, including those prepared from polyolefins, is due to the demand of materials with improved properties. The purpose of adding mineral fillers to polymers was primarily one of the cost reductions but recently, the fillers have been more often used to fulfill a functional role, such as increasing stiffness or improving the dimensional stability of the polymer [1]. The fillers affect ultimate mechanical properties in two ways: (i) they act directly as harder particles with determined properties (shape, size, and modulus) and (ii) they affect crystallization processes in polymer matrix and ultimate supermolecular structure of semicrystalline polymer.

Commonly used mineral fillers for isotactic polypropylene (iPP) include talc, calcium carbonate, glass fibers, and wollastonite. Because of its acicular crystal habit and a relatively high-level hardness, wollastonite ($CaSiO_3$—calcium metasilicate) contributes to the iPP composites reinforcing properties [2–4]. Although different authors have reported a wide spectrum of results on how wollastonite affects mechanical properties, supermolecular structure of binary iPP/wollastonite composites, as well as those modified by impact modifiers, coupling agents or compatibilizers have been rarely investigated [5–8]. The addition of components such as iPP-*g*-MA or EPDM improves impact strength and affects final morphology. It has been proved that EPDM tercopolymer preferably incorporates in the iPP matrix in the form of dispersed particles rather than that it encapsulates wollastonite filler because of stronger interactivity or similarity with the iPP matrix [8]. These polypropylene based copolymers are replaced by styrenic rubber block copolymers (SRBC), in order to achieve better encapsulation of wollastonite particles. According to this aim, the effects of the incorporation of wollastonite, as well as two comparable elastomers (SEBS and SEBS-*g*-MA block copolymers) on final structure of the iPP/wollastonite/SRBC composites are discussed in this paper, while the mechanical performance of these composites will be presented in another paper.

EXPERIMENTAL

Materials

The materials used in this study were isotactic polypropylene (iPP), two types of wollastonite and two types of block copolymers (SEBS, SEBS-*g*-MA). The iPP used for sample preparation was Moplen HP501L, Basell (melt

Correspondence to: Ivan Šmit; e-mail: ismit@irb.hr
Contract grant sponsors: Ministry of Higher Education, Science, and Technology, Republic of Slovenia; Ministry of Science, Education, and Sports, Republic of Croatia; contract grant number: 098-0982904-2955.
DOI 10.1002/pen.20899
Published online in Wiley InterScience (www.interscience.wiley.com).

flow rate [MFR] = 6 g/10 min, ρ = 0.90 g/cm^3, M_n = 120,000 g/mol). Applied mineral fillers were proprietary (combination of silanes) surface treated wollastonite (W1) Tremin 939 300 ZST, Quarzwerke (ρ = 2.85 g/cm^3, specific surface 1.2 m^2/g, d(50%) = 9 μm) and wollastonite surface treated with aminosilane (W2) Tremin 939 300 AST, Quarzwerke (ρ = 2.85 g/cm^3, specific surface 1.2 m^2/g, d(50%) = 9 μm). Styrenic block copolymers poly (styrene-*b*-ethylene-*co*-butylene-*b*-styrene) (SEBS) Kraton G-1652, Kraton Polymers ([MFR] = 0.5 g/10 min, ρ = 0.91 g/cm^3, M_n = 65,900 g/mol) and poly(styrene-*b*-ethylene-*co*-butylene-*b*-styrene) grafted with maleic anhydride (SEBS-*g*-MA) Kraton KG-1901, Kraton Polymers ([MFR] = 3.1 g/10 min, ρ = 0.91 g/cm^3, M_n = 47,300 g/mol) were used as elastomers.

Sample Preparation

Binary iPP/wollastonite and ternary iPP/wollastonite/elastomer composites were prepared in an oil-heated Brabender kneading chamber. The iPP/wollastonite ratio was kept constant at 92/8 vol% and the elastomer of 2.5, 5, 10, and 20 vol% was added. The components were put into a chamber preheated up to 200°C with a rotor speed of 50 min^{-1}. The components were kneaded for 7 min. After homogenization, the melt was rapidly transferred to a preheated laboratory press and compression molded into 1- and 4-mm-thick plates. The pressing temperature was 220°C, pressure 100 bar and the pressing time of 14 min for 1-mm and 11.5 min for 4-mm-thick plates. Afterwards, the plates were cooled to room temperature in the air.

Optical Microscopy

A Leica light microscope (Model DMLS) with digital camera was used for thin crossed microtomed sections (1-mm-thick plates) observations.

Scanning Electron Microscopy

A Jeol JSM-840A scanning electron microscope (SEM) was used for studying the morphology of the investigated composites. The samples were fractured in liquid nitrogen and covered with gold before being examined by a microscope at an acceleration voltage of 5 kV by 1000× and 3000× magnification. Xylene was used for etching the elastomeric phase in order to obtain better examination of distributed elastomeric particles in composites. All SEM micrographs are secondary electron images.

Transmission Electron Microscopy

Ultrathin sections (75–85-nm thick) were cut from 4-mm-thick plates with Leica- Ultracut E microtome equipment with a diamond knife. Before microtoming, samples were exposed to RuO_4 to contrast and harden the samples. Microtomed ultrathin sections were then collected on copper grids and micrographs were taken at an acceleration voltage of 100 kV by a Tecnai G^2 12 microscope with CCD camera (Gatan Bioscan).

Wide-Angle X-Ray Diffraction

The wide-angle X-ray diffractograms of rotated samples (1-mm-thick plates) were taken by a Philips diffractometer with monochromatized CuK_α radiation in the diffraction range of 2θ = 5–40°. A degree of crystallinity, $w_{c,x}$, was evaluated by the Hermans-Weidinger method [9]. The crystallite size L_{110} was calculated by Scherrer formula [10] from half-maximum width of *110* α-iPP reflection and B value (earlier known as K value) [11], as a measure for hexagonal β-form content, was calculated by formula (1) proposed by Zipper et al. [12]:

$$B = \frac{I_{\beta-300}}{I_{\beta-300} + I_{110} + I_{040} + I_{130}} \tag{1}$$

where, I represents the intensities of the corresponding reflections.

The orientation parameters A_{110} and C used as measures for orientations of corresponding (110) and (040) planes were calculated by formulae proposed by Zipper et al. [12]:

$$A_{110} = \frac{I_{110}}{I_{110} + I_{111} + I_{\bar{1}31+041}} \tag{2}$$

$$C = \frac{I_{040}}{I_{110} + I_{040} + I_{130}} \tag{3}$$

where, I represents the intensities of the corresponding reflections.

Differential Scanning Calorimetry

Thermal analysis was performed with a PerkinElmer DSC-7 calorimeter. The samples (9.3–10.3 mg) were cut from 1-mm-thick compression molded plates, placed in aluminium pans and sealed. The instrument was operated in a dynamic mode. First, the samples were heated to 180 C with a controlled heating rate of 10°C/min in extra pure nitrogen environment and then kept at that same temperature for 5 min [13]. Thermograms were recorded during the cooling cycle with a cooling rate of 5°C/min to 25°C, as well as by second heating to 180°C with a heating rate of 10°C/min. The melting temperatures, T_m, of samples were obtained from the maximum of the second melting peaks and enthalpies of melting, Δh, were obtained from the peak area and recalculated on iPP mass. The crystallinity, $w_{x,h}$, of iPP and of the composites was calculated by *Eq. 4*:

$$w_{c,h} = \frac{\Delta h}{\Delta h^0_{PP}} \times 100 \tag{4}$$

 DOI 10.1002/pen

where, Δh was the enthalpy of fusion per gram of the sample recalculated on iPP mass and Δh^{o}_{PP} was the enthalpy of fusion per gram of 100% crystalline iPP. For Δh^{o}_{PP}, the value of 148 J/g was used [14].

Following quantities were given from crystallization exotherm and were related with crystallization parameters [13].

i. The peak temperature of the exotherm, T_c.
ii. The temperature of the onset of crystallization, T_{onset}, is the temperature where the crystallization process begins.
iii. Slope of the exotherm, S_i, which is the slope of the high temperature side of the exotherm.
iv. The quantity $T_i - T_c$. T_i is an intercept of the tangent at high temperature side of the exotherm with the baseline.
v. The width at half-height of the exotherm peak, Δw.

RESULTS AND DISCUSSION

Phase Morphology

Optical Microscopy. Typical morphologies of examined samples are presented with polarization micrographs of pure iPP and binary iPP/W2 composite shown in Fig. 1. The micrograph of pure iPP reveals uniform, well-developed spherulitic morphology with radial, polygonal, and flower-like spherulites. The incorporation of both wollastonite types into iPP matrix disturbs regular spherulitization. Polarization micrographs of binary composites reveal morphology with thin, dark branched iPP grains without the Maltese cross (Fig. 1b). Obviously, thin needle-like wollastonite particles strongly affect nucleation of the iPP matrix and thus, hinder a well-developed spherulitization in the iPP matrix. Additionally, the spherulite growth may be restrained at particles surface of filler according to Burke et al. [15]. Dispersed elastomer (SEBS and SEBS-*g*-MA) particles affect crystallization of the iPP matrix by nucleation and solidification effect and thus, influence their final spherulitic morphology [13, 16–20]. Even separated SEBS particles in the iPP/SEBS blends with lower SEBS amount (up to 5%) [13, 19] have revealed nucleation ability due to interactive SEBS–iPP interface [16] or good interfacial adhesion or due to active micellar clusters in SEBS particles (up to 10 wt%) [17, 18]). Although the addition of higher amounts of SEBS and SEBS-*g*-MA to pure iPP or iPP/W composites may enhance spherulitization [8, 20], regular spherulites in ternary iPP/W/SRBC composites were not recognizable in microscopy under crossed polars, even at 20 vol% of added SRBC.

Optical and polarization micrographs of all composites reveal homogenous distribution of separated wollastonite particles without agglomeration (Fig. 2). Wollastonite crystals in binary iPP/W and ternary iPP/W/SEBS composites orientate preferentially plane-parallel to the compression-molded surface. The addition of SEBS to the iPP/W composites maintains this plane-parallel orientation in irregular way (the orientation somewhat varies through the sample as shown inserted picture in micrograph of this composite in Fig. 2b). Contrary, the addition of SEBS-*g*-MA causes evident disorientation of wollastonite particles in the iPP matrix (Fig. 2c). Stronger disorientation of acicular wollastonite particles in the composites with SEBS-*g*-MA may be caused by stronger wollastonite–SEBS-*g*-MA interactions than those of wollastonite–SEBS interactions.

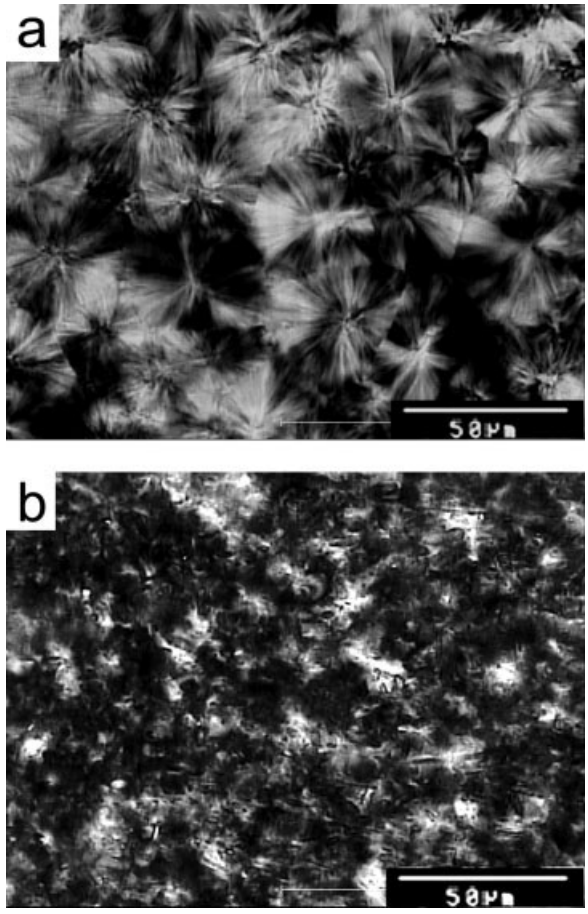

FIG. 1. Polarizing micrographs of (a) pure iPP and (b) the iPP/W2 92/8 composite.

Scanning Electron Microscopy. Scanning electron micrographs of fractured iPP/wollastonite composites with 20 vol% of added SEBS and SEBS-*g*-MA are presented in Fig. 3. SEM micrographs confirm homogeneous distribution of wollastonite without agglomeration and also homogeneously dispersed SRBC particles in the iPP matrix. Needle-like wollastonite particles orientate preferentially in the melt flow direction during the compression molding of the sample into a plate. There are major differences in microphase morphology of composites with different SRBC elastomers if compared with those with different wollastonite types. The micrographs reveal the presence of a larger number of wollastonite crystals with

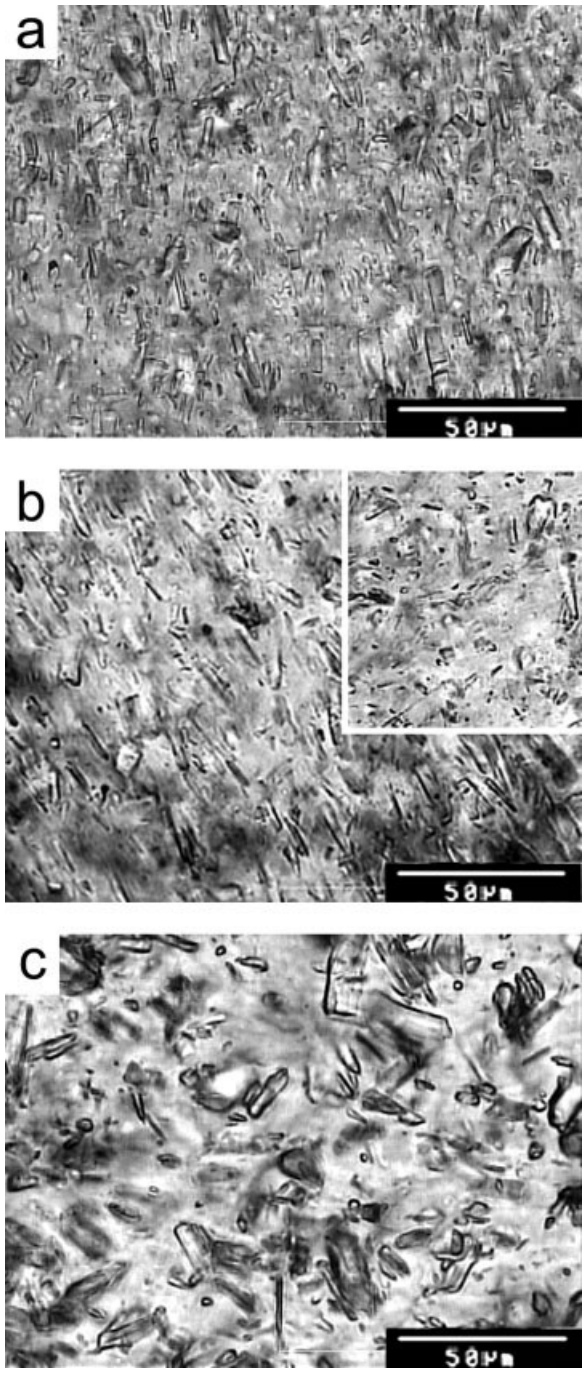

FIG. 2. Optical micrographs of (a) the iPP/W2 92/8 composite and the iPP/W2 92/8 composite with (b) 20 vol% of SEBS and (c) 20 vol% of SEBS-*g*-MA.

higher plane-parallel orientation at etched surface of binary iPP/wollastonite and ternary composites with SEBS (Fig. 3a and b) than in those with the SEBS-*g*-MA elastomer (Fig. 3c). The comparison of micrographs indicates more frequent and more expressive encapsulation of wollastonite particles by the SEBS-*g*-MA than by the SEBS interlayers (Fig. 3). The complete encapsulation of wollastonite particles by the elastomer could be hindered due to the wollastonite distinct acicular form with higher aspect ratio in regard to other fillers. In spite of observed more expressive encapsulation of wollastonite by SEBS-*g*-MA than that by SEBS, the fractured surface of iPP/W/SEBS-*g*-MA composite with more pulled out wollastonite particles than those from surface of the iPP/W/SEBS composite (apparently confront this interpretation), could be explained by other reasons: (i) wollastonite particles could be pulled out more easily from thicker and softer SEBS-*g*-MA (lower viscosity of SEBS-*g*-MA than SEBS) than from rare thin SEBS interlayers; (ii) wollastonite particles are tougher constrained in the iPP matrix (prevalently in

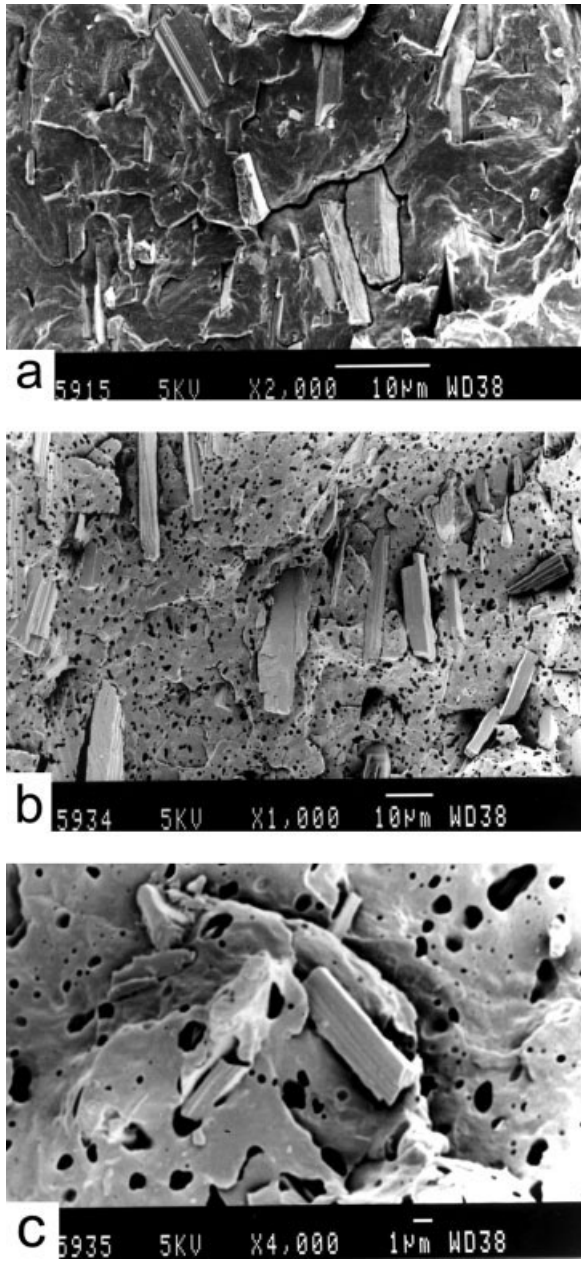

FIG. 3. SEM micrographs of the fractured surfaces of composites: (a) iPP/W1 92/8, (b) iPP/W1 92/8 with 20 vol% of SEBS, and (c) iPP/W1 92/8 with 20 vol% of SEBS-*g*-MA.

 DOI 10.1002/pen

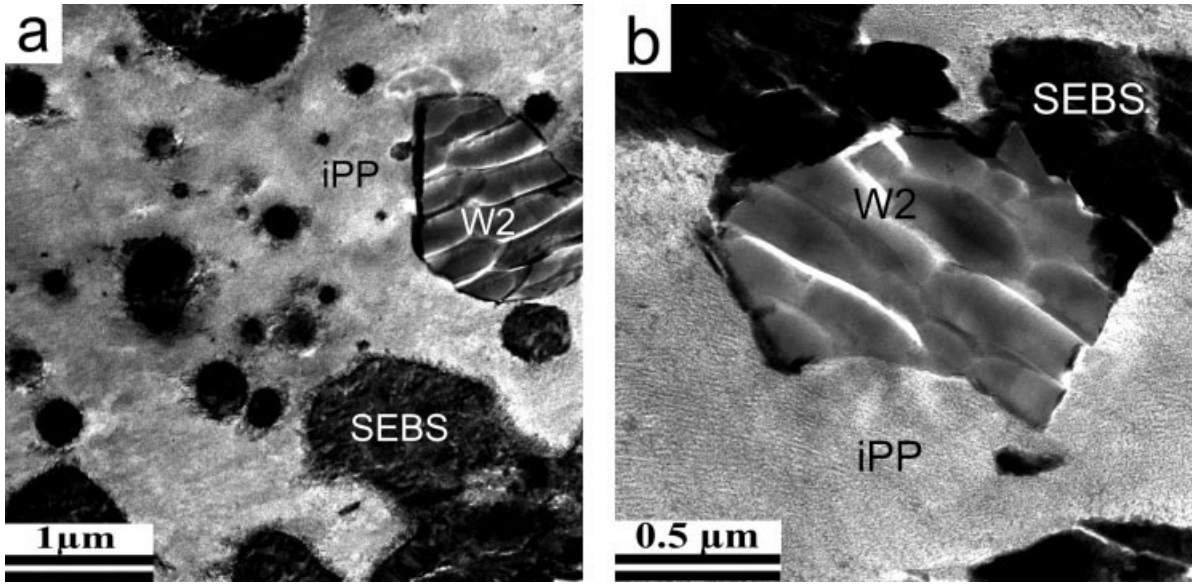

FIG. 4. Transmission electron micrographs of the iPP/W2 92/8 composite with 20 vol% of SEBS reveal mostly (a) W2 particles alongside of dispersed SEBS particles and (b) partly encapsulated W2 particles.

the case of iPP/W/SEBS composites) than those in the SEBS-*g*-MA interlayers.

Transmission Electron Microscopy. Ternary polymer/filler/elastomer composites exhibit two characteristic microphase morphologies with respect to location of filler and elastomer particles in polymer matrix [16]: (i) separated microphase morphology where elastomer and filler particles are randomly dispersed in polymer matrix (apart from each other), and (ii) core-shell morphology where the filler particles are encapsulated by the elastomer. However, the most frequent morphology observed for various composites consists of a combination of two main morphologies [16]. TEM micrographs in Figs. 4 and 5 revealed a combination of these two morphologies in ternary iPP/W/SRBC composites. Actually, the iPP/W/SEBS composites show a variety of morphologies from separated wollastonite particles in the iPP matrix over most frequently accommodated alongside of SEBS particles (i.e. located between iPP matrix and SEBS) (Fig. 4a) to partly or completely encapsulated by SEBS (Fig. 4b). Unlike iPP/W/SEBS composites, TEM micrographs of composites with SEBS-*g*-MA, reveal greater number of wollastonite particles partly or completely encapsulated

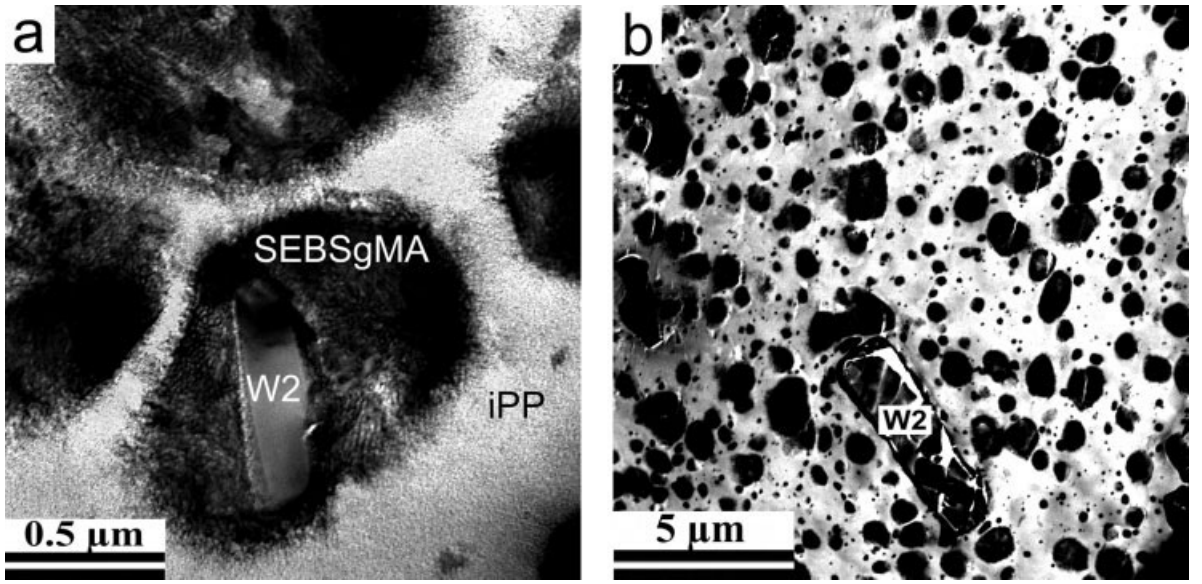

FIG. 5. Transmission electron micrographs of the iPP/W2 92/8 composite with 20 vol% of SEBS-*g*-MA with (a) higher and (b) lower magnification.

by SEBS-*g*-MA elastomer as shown in Fig. 5a (i.e. the variety of morphologies is shifted to higher extent of core-shell morphology). Lower magnification of TEM micrographs also reveals separately dispersed elastomer particles in the iPP matrix in composites with SEBS-*g*-MA (Fig. 5b).

TEM and SEM micrographs confirmed encapsulation efficiency of polar SEBS-*g*-MA higher than that of SEBS elastomer. Just a few papers on core-shell morphology of ternary composites attempted to explain filler encapsulation by influencing factors, i.e. by (i) conditions during the preparation of the composites [21] and (ii) nature of compatibilizer such as unsaturated (SBS, SIS) or polar elastomers (SEBS-*g*-MA) that encapsulate fillers more easily in comparison with those saturated (EPDM, EPR, SEBS) forming thus core-shell morphology according to the presumption of Stamhuis [22]. Stricker et al. [18] and Denac et al. [19] confirmed this hypothesis showing that encapsulation of talc particles by SEBS-*g*-MA was favored by polarity if compared with SEBS. Higher encapsulation efficiency of polar SEBS-*g*-MA, if compared with that of SEBS elastomer, found in this work could be explained by interactions between SEBS-*g*-MA–aminosilanes coupling agent, which could be stronger than those of SEBS–aminosilanes at wollastonite surfaces. The results based on contact angle measurements confirm stronger SEBS-*g*-MA–wollastonite interactions than those of SEBS–wollastonite, because of higher work of adhesion value at SEBS-*g*-MA–wollastonite (W_{mf} = 99.4 mJ/m^2 for SEBS-*g*-MA/W2) than that of at SEBS–wollastonite (W_{mf} = 87.1 mJ/m^2 for SEBS/W2) interface [20, 23]. Obviously, the difference in microphase morphology arises from the differences between SEBS-*g*-MA–W and SEBS–W interactions, since the values of adhesion work of the iPP/W1 and iPP/W2 composites as well as for the iPP/elastomer interfaces are similar [20, 23]. As a result of stronger SEBS-*g*-MA–aminosilanes interactions and encapsulation of wollastonite particles, the addition of SEBS-*g*-MA elastomer to the iPP/W composites disorients wollastonite particles more significantly. Although both elastomers cause a combined morphology (separated and core-shell) [16], a significant difference in microphase morphology of composites with SEBS and SEBS-*g*-MA could be deduced. Both elastomers are as separate particles predominantly dispersed in the iPP matrix. Closely situated wollastonite and dispersed SEBS particles (filler particles seem to accommodate alongside of SEBS particles or layers, whereas filler locates between the iPP matrix and SEBS) give an impression that wollastonite particles are partly overlapped by SEBS. Actually, both SEBS and wollastonite are embedded into the iPP matrix. In composites with SEBS-*g*-MA, wollastonite particles are embedded into SEBS-*g*-MA particles in higher extent (Fig. 5a) and SEBS-*g*-MA acts as an interlayer between wollastonite particles and the iPP matrix (Fig. 5b). Generally, composites with SEBS-*g*-MA overwhelmingly exhibit a core-shell morphology.

Phase Characteristics

Phase Structure. X-ray diffractogram of pure iPP exhibits solely stable monoclinic α-form, whereas, apart from α-form, the diffractograms of composites reveal small amounts of hexagonal β-form of crystalline iPP phase (as shown in Fig. 6). It is known that wollastonite affects the β-nucleation in iPP [5]. Relatively low content of β-phase (with B or K values for measuring β-form content being 0.02–0.06) in the iPP/W/SRBC composites (Fig. 7) in comparison with binary iPP/W composites (K = 0.14 for composite with 3.2% of wollastonite [5]) might arise from partial encapsulation of wollastonite particles performed by SRBC elastomer. On the other hand, SEBS copolymer promotes α-nucleation of iPP matrix [13, 20]. One might assume that overlapping of wollastonite particles as a β-nucleator by SEBS and SEBS-*g*-MA reduces β-form content of iPP. The β-form content in composites with SEBS-*g*-MA (composites with higher degree of encapsulation), which is lower than that in composites with SEBS, seems to confirm this conclusion (Fig. 7). Diffractograms of both applied wollastonites are closer to the Card No. 27-1064 (triclinic cell with space group P$\underline{1}$ (2T)) [24] than to the Card No. 19-249 (triclinic cell with space group P1 (1T)) [25].

Crystallinity and Crystallite Size. The overall degree of crystallinity has been calculated [9] as a crystalline fraction (α- plus β-iPP phase) in total polymer fraction

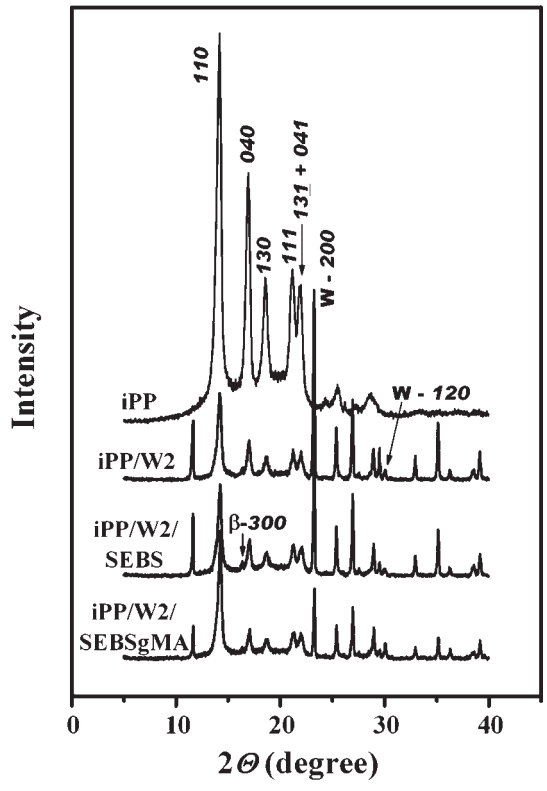

FIG. 6. Diffractograms of the iPP, binary iPP/W2 92/8 composite and ternary composites with 20 vol% of SEBS and SEBS-*g*-MA elastomers.

 DOI 10.1002/pen

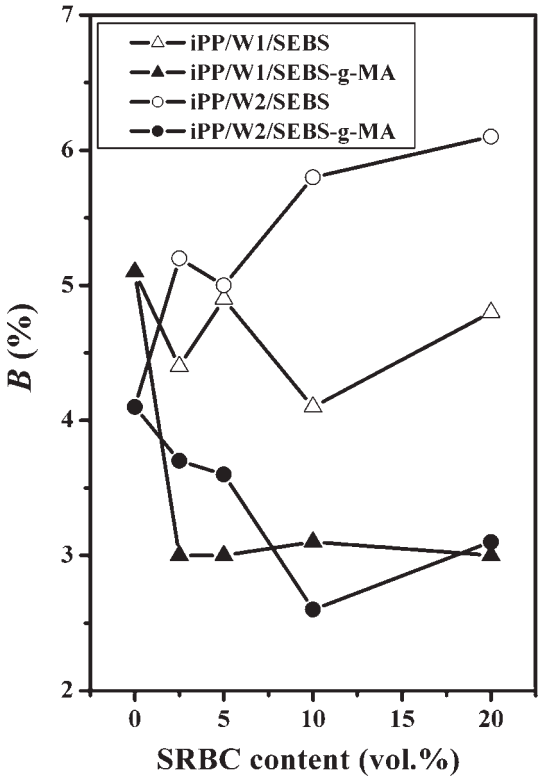

FIG. 7. B parameter (as a measure for β-iPP content) of composites as a function of SRBC content.

(iPP plus SRBC) in ternary composite following the Hermans-Weidinger method. The crystallinity calculation has taken into account total polymer fraction (iPP plus SRBC), since main diffuse diffraction maximum is common maximum of two overlapping broad maxima of the iPP and SRBC amorphous phases in the diffraction angle range of $2\theta = 7$–32°. The crystallinity values are recalculated on the pure iPP, to compare them with those obtained from the enthalpy of fusion per gram of the sample recalculated on iPP mass. The evaluated crystallinity values, $w_{c,x}$, increase to some extent upon incorporation of wollastonite filler in pure iPP (Fig. 8). This effect is in accordance with the observation referred to by Wypich [1]. It seems that the crystallinity increases with an increase in SRBC elastomers content as shown by multiple fitting line in Fig. 8. The increasing of the β-iPP content, due to β-nucleation ability of wollastonite, may contribute to the overall crystallinity increase. However, other effects may additionally contribute to this increase: (i) dissolution of amorphous iPP and SRBC phases by wollastonite, (ii) prolonged crystallization due to solidification effect of SRBC elastomer, and (iii) limiting resolution of applied method.

The crystallite size, L_{110}, exhibits similar, even stronger increase with the increasing SRBC content as shown by multiple fitting line in Fig. 9. At lower amount of SRBC, the small-dispersed SRBC particles may increase the heterogeneous nuclei density and decrease the crystallite size. A steady increase of the L_{110} crystallite size

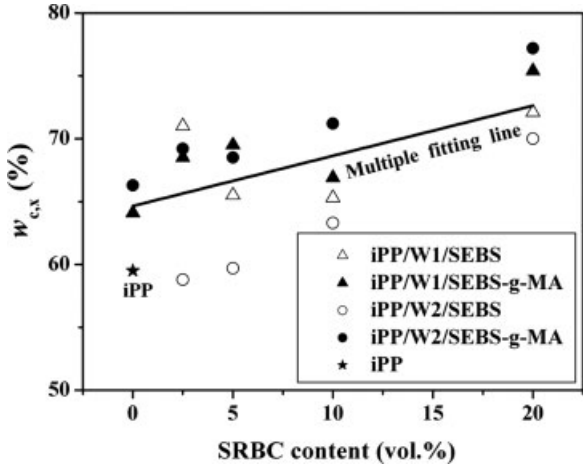

FIG. 8. Overall degree of crystallinity, $w_{c,x}$, of composites recalculated on polypropylene mass unit as a function of SRBC content.

upon further addition of SRBC might be ascribed to the solidification effect, which prolongs crystallization of the iPP matrix, as well as to the easier migration of iPP chains transferred by SRBC melt during the crystallization process. The solidification effect obviously prevails over the SRBC nucleation effect and, consequently, enhances crystal growth.

Orientation. The incorporation of wollastonites and SRBC elastomers into iPP matrix affects the intensities of α-iPP reflections as indicated in Fig. 6. As a consequence, the ingredients affect the values of A_{110} and C parameters as an orientation measure for α-form crystallites in plane-parallel to the sample surface. Only the incorporation of the W2 filler in the iPP matrix intensifies the 110 reflection (A_{110} parameter in Fig. 10), whereas both wollastonites depress the 040 reflection (C parameter in Fig. 11). SEBS and SEBS-g-MA affect A_{110} and C values in a more distinguished manner than both wollastonites. The change in the values with SRBC content is more regular in composites with the W2 filler. The addition of SEBS

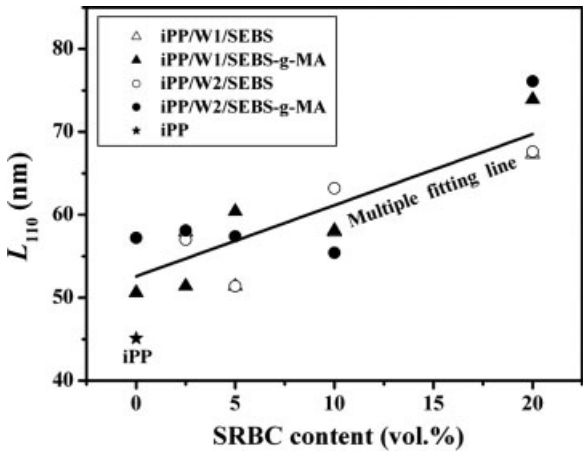

FIG. 9. Crystallite size, L_{110}, as a function of the SRBC content.

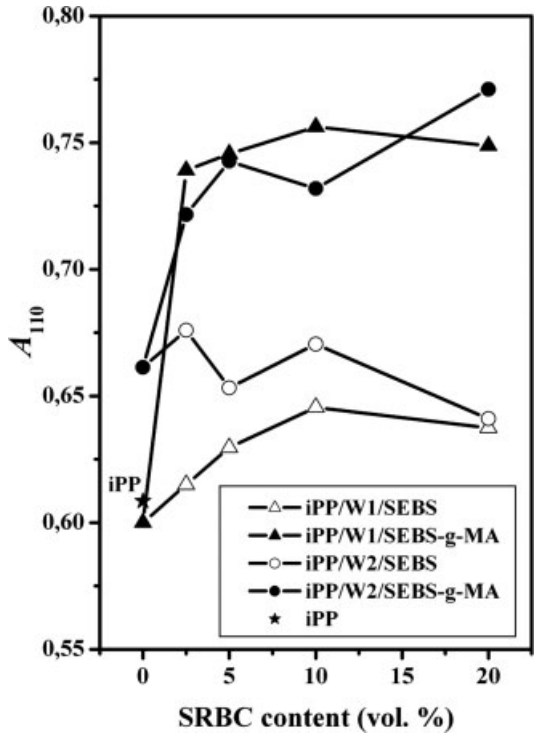

FIG. 10. Orientation A_{110} parameter as a function of the SRBC content.

affects A_{110} and C values slightly or irregularly. For distinct-to-slight reorientation effect caused by SEBS, already a minor amount of SEBS-*g*-MA (2.5 vol%) causes a significant increase in A_{110} parameter (Fig. 10), and a decrease in C value (Fig. 11). Obviously, polar SEBS-*g*-MA elastomer affects the orientation of α-iPP crystallites much stronger than that of wollastonites, but it does it in the same direction. The intensifying of the 110 reflection ($A_{110} = 0.72$–0.74) upon an addition of SEBS-*g*-MA indicates the increased number of (110) planes in planes parallel to the sample surface. That indicates a presumable tilting of the α-iPP lamellae with fold plane (010) to the sample surface. On the other hand, very low C values (up to 0.10–0.15) might be explained, according to Zipper et al. [12], by maintaining either c-axial orientation or isotropic iPP matrix ($0 < C \ll 1$ for pure c-axis orientation or for isotropic material). According to Fujiyama et al. [26], c-axis-oriented lamellae imply orientation of macromolecular c-axis, lying in the planes parallel to the sample surface in machine direction.

Observed by optical and SEM microscopy, the plane-parallel orientation of wollastonite particles manifests in the change of intensity of some wollastonite reflections in the diffractograms of composites in comparison with pure wollastonite (see Fig. 6). The increase of intensity relationship of 200 and 120 reflection, I_{200}/I_{120}, in iPP/W composites in comparison with pure wollastonite (W* in Fig. 12), confirms the preferential orientation of wollastonite crystals incorporated into the iPP matrix. This relationship varies upon an addition of SEBS to composites, but global trend of the I_{200}/I_{120} values, i.e. preferential orientation of wollastonite, remains unchanged. Opposite to SEBS, the SEBS-*g*-MA elastomer reduces this value to

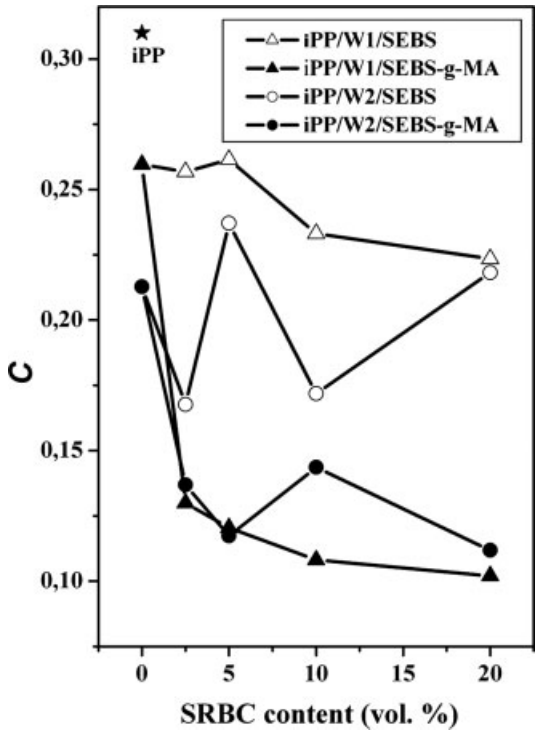

FIG. 11. Orientation C parameter as a function of the SRBC content.

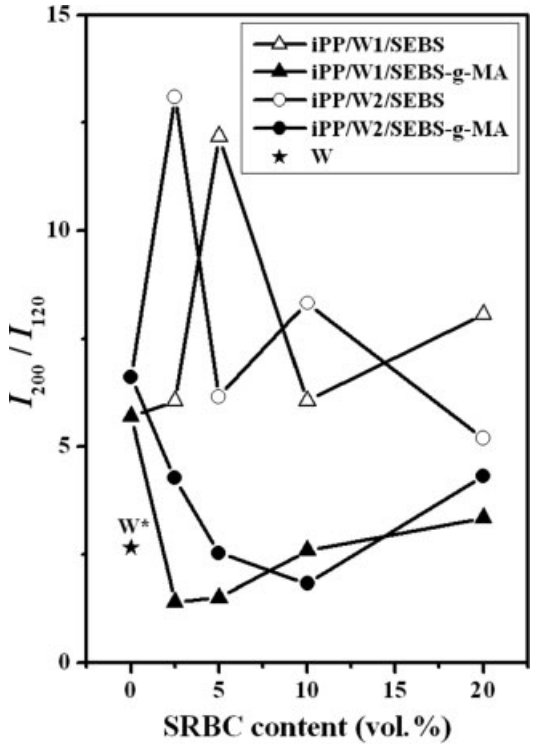

FIG. 12. Intensity relationship I_{120}/I_{200} of wollastonite reflections as a function of the SRBC content.

DOI 10.1002/pen

the value for pure wollastonite (W* in Fig. 12). In other words, the SEBS-*g*-MA elastomer disorients wollastonite particles more strongly than the SEBS elastomer does. This fact is in good accordance with higher encapsulation ability of the SEBS-*g*-MA elastomer.

Thermal Properties. The melting temperature of α-iPP crystallites in composites varies negligibly in comparison with the pure iPP ($T_m = 165^\circ C$). Obviously, neither wollastonite filler nor SRBC elastomer affect significantly the melting peak temperature of α-iPP. The behavior of crystallinity values, $w_{c,h}$, obtained from the DSC measurements is similar to those values, $w_{c,x}$, calculated from WAXD diffractograms. The addition of SRBC elastomers somewhat increases the degree of crystallinity (Fig. 13). Such behavior of crystallinity confirms that the solidification effect prevails over the nucleation effect upon an increase in the amount of added SRBC elastomers.

The crystallization behavior of composites has been deduced from the quantities given from crystallization exotherms. Because of relatively narrow crystallization peaks of all samples, the determined values of exotherm slopes, S_i, the quantity $T_i - T_c$ and width at half-height of the exotherm, Δw, could not prove valuable conclusions. Sharp slope, S_i, and low $T_i - T_c$ differences of the exotherms imply a relatively fast nucleation as well as great overall rate of crystallization. A slight decrease in half-peak width of pure iPP ($\Delta w = 13.2^\circ C$) upon an introduction of fillers and elastomers ($\Delta w = 11$–$13^\circ C$) might be caused by slight decrease in crystallites size distribution. However, the enthalpy of crystallization, peak temperature of crystallization exotherm (crystallization temperature), T_c, and temperature of onset of crystallization, T_{onset}, change discernible upon an incorporation of wollastonite and SRBC elastomers. The enthalpy of crystallization changes with SRBC addition similarly to the enthalpy of melting as presented with crystallinity values in Fig. 13. The onset of crystallization, T_{onset}, and the crystallization

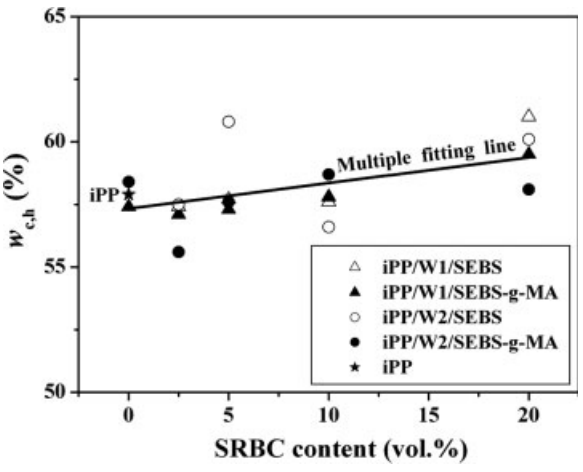

FIG. 13. Overall degree of crystallinity, $w_{c,h}$, of composites recalculated on polypropylene mass as a function of SRBC content.

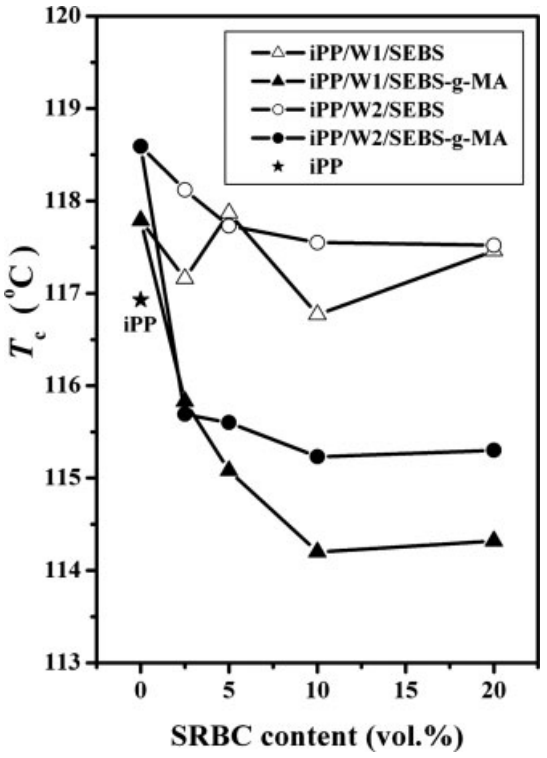

FIG. 14. Crystallization temperature (T_c) as a function of SRBC content.

temperature, T_c, change similarly upon the incorporation of fillers and elastomers. Both wollastonites increase their T_c values (Fig. 14). This is in accordance with the observed nucleation effect of filler [4], i.e. wollastonite particles increase the heterogeneous nuclei density and, thus, accelerate and promote the crystallization of the iPP. The SEBS elastomer affects the temperature of crystallization negligibly, whereas the addition of SEBS-*g*-MA elastomer decreases T_c systematically (Fig. 14) similarly as the β-iPP content (*B* values in Fig. 7) and the orientation *C* parameter (Fig. 11). This behavior is in a good agreement with the finding of Fujiyama that the crystallization temperature increases with an increase in β-iPP content (actually with γ-quinocridone content) [27]. The observed number of SEBS-*g*-MA greater than that of SEBS interlayers in iPP composites separates wollastonite particles from iPP matrix in higher extent thus reducing the β-iPP nucleation ability of wollastonite.

CONCLUSION

The wollastonite particles are homogeneously incorporated into the iPP matrix without aggregation and oriented plane-parallel to the sample surface. The wollastonite filler disturbed a well-developed spherulitization of iPP. Both block copolymers (SEBS and SEBS-*g*-MA) affected the crystallite size and degree of crystallinity, i.e. the crystallization of iPP matrix mainly by solidification effect. The encapsulation of wollastonite particles was

more expressed by SEBS-*g*-MA than by SEBS elastomer. In spite of more extensive core-shell morphology in iPP/wollastonite/SEBS-*g*-MA than that in iPP/wollastonite/SEBS composites, the fractured surfaces of composites with SEBS elastomer showed more though fracture. On the other hand, the introduced SEBS-*g*-MA elastomer in forms of interlayers or dispersed particles affected the orientation of wollastonite particles and iPP crystals more significantly than SEBS elastomer did. The SEBS-*g*-MA elastomer disorientated plane-parallel wollastonite particles and induced c-axis-oriented α-iPP lamellae. The SEBS-*g*-MA elastomer, as an active component, interacted with the iPP chains and reduced their mobility, diffusion, as well as the temperature of crystallization of oriented α-iPP lamellae. All changes observed were more regularly in composites with the W2 wollastonite, i.e. with wollastonite treated with aminosilane only.

ACKNOWLEDGMENTS

The authors thank Mr. J. Pohleven for his help in the experimental work, Dr. E. Ingolič for her valuable help in elaborating the TEM micrographs, and Dr. N. Filipović-Vinceković for useful advices when writing this article.

REFERENCES

1. W.C.J. Zuiderduin, C. Westzaan, J. Huetink, and R.J. Gaymans, *Polymer*, **44**, 261 (2003).
2. J.H. Kietzman, "Asbestiform Fillers," in *Additives for Plastics*, *Vol. 1*, R.B. Seymour, Ed., Academic Press, New York, 51 (1978).
3. R.N. Rothon, *Adv. Polym. Sci*., **139**, 67 (1999).
4. G. Wypich, *Handbook of Fillers*, SPE, New York, 167 (1999).
5. J. Liu, X. Wei, and Q. Guo, *J. Appl. Polym. Sci*., **41**, 2829 (1990).
6. D.H. Roberts, In *Proceedings of SPE ANTEC*, Atlanta, USA, 1427 (1998).
7. J. Chu, C. Xiang, H.-J. Sue, and R.D. Hollis, *Polym. Eng. Sci*., **40**, 944 (2000).
8. I. Šmit, V. Musil, and I. Švab, *J. Appl. Polym. Sci*., **91**, 4072 (2004).
9. P.H. Hermans and S.A. Weidinger, *Makromol. Chem*., **50**, 98 (1961).
10. L.E. Alexander, *X-Ray Diffraction Methods in Polymer Science*, Wiley, New York, 423 (1969).
11. A. Turner-Jones, J.M. Aizlewood, and D.R. Becket, *Makromol. Chem*., **75**, 134 (1964).
12. P. Zipper, A. Janosi, E. Wrentschur, C. Knabl, and P.M. Abuja, *Österr. Kunststoff-Zeitschrift*, **24**, 162 (1993).
13. A.K. Gupta and S.N. Purwar, *J. Appl. Polym. Sci*., **29**, 1595 (1984).
14. B. Monasse and J.M. Haudin, "Molecular Structure of Polypropylene Homo- and Copolymers," in *Polypropylene: Structure Blends and Composites, Vol. 1, Structure and Morphology*, J. Karger-Kocsis, Ed., Chapman and Hall, London, Chapter 1 (1995).
15. M. Burke, R.J. Young, and J.L. Stanford, *Plast. Rubber Compos. Process. Appl*., **20**, 121 (1993).
16. Y. Long, R.A. Shanks, and Z.H. Stachursky, *Prog. Polym. Sci*., **20**, 651 (1995).
17. U. Plawky and W. Wenig, *Macromol. Symp*., **102**, 183 (1996).
18. F. Stricker and R. Mülhaupt, *High Perform. Polym*., **8**, 97 (1996).
19. M. Denac, I. Šmit, and V. Musil, *Compos. A*, **36**, 1094 (2005).
20. I. Švab, The Study of Modification of Isotactic Polypropylene with Wollastonite and Elastomers, Ph.D. Thesis, University of Maribor, Maribor, Slovenia (2006).
21. Y.C. Ou, T.T. Guo, X.P. Fang, and Z.Z. Yu, *J. Appl. Polym. Sci*., **74**, 2397 (1999).
22. J.E. Stamhuis, *Polym. Compos*., **9**, 280 (1988).
23. I. Švab, V. Musil, and M. Leskovac, *Acta Chim. Slov*., **52**, 264 (2005).
24. ICDD, JCPDS, *Powder Diffraction File*, Swarthmore, PA, Card No. 27-1064.
25. ICDD, JCPDS, *Powder Diffraction File*, Swarthmore, PA, Card No. 19-249.
26. M. Fujiyama, T. Wakino, and Y. Kawasaki, *J. Appl. Polym. Sci*., **35**, 29 (1988).
27. M. Fujiyama, *Int. Polym. Process*., **10**, 172, 251 (1995).

 DOI 10.1002/pen